First Principles Investigation of the Stability and the Chemical Behavior of Hydrogen in $ThCoH_4$

Samir F. Matar

CNRS, Université de Bordeaux, ICMCB, 87 avenue du Docteur Albert Schweitzer, F-33608 Pessac, France

Reprint requests to Samir F. Matar. E-mail: matar@icmcb-bordeaux.cnrs.fr

Z. Naturforsch. **2011**, *66b,* 269 – 274; received December 3, 2010

We address the changes in the electronic structure brought by the insertion of hydrogen into ThCo leading to the experimentally observed $ThCoH_4$. Full geometry optimization positions the hydrogen in three sites stabilized in the expanded intermetallic matrix. From a Bader charge analysis, hydrogen is found to be in a narrow iono-covalent (~ -0.6) to covalent (~ -0.3) bonding which should enable site-selective desorption. The overall chemical picture shows a positively charged $Th^{\delta+}$ with the negative charge redistributed over a complex anion $\{CoH_4\}^{\delta-}$ with $\delta \sim 1.8$. Nevertheless this charge transfer remains far from the one in the more ionic hydridocobaltate anion $CoH_5{}^{4-}$ in Mg_2CoH_5, due to the largely electropositive character of Mg.

Key words: ThCo Intermetallic, DFT, CrB Type, Hydrides, Bader Charge, Chemical Bonding

Introduction

Equiatomic (1 : 1) nickel-based binary intermetallic compounds such as *A*Ni with *A* = Y, Zr, Hf and rare earths (*RE*) [1–3] have been studied extensively both experimentally and theoretically in recent years mainly for their ability of absorbing hydrogen with up to three atoms per formula unit (fu) under mild conditions. On the other side, among the smaller number of cobalt 1 : 1 compounds, the hydrogen uptake within ThCo amounts to more than 4 atoms per fu (4.2) [4,5]. Such a result is interesting in as far as it resembles those in recent reports on a high hydrogen content in *RE*Ni leading to $RENiH_4$ [2]. For ThCo, this leads to $\sim$ 1.4 wt.-% hydrogen instead of 3 wt.-% for hydrogenated *A*Ni with the lighter *A* elements. Nevertheless, low weight percentages were also found in hydrogenated C15b pseudo-Laves hydrides such as $REMgNiH_4$ considered as candidates for on-board hydrogen storage [6]. Note that the use of the term "hydrogenated system" rather than "hydride system" is intended to differentiate covalently bonded hydrogen within the intermetallic compound with respect to ionic hydrides such as those based on alkali and alkaline earth metals (*cf.* [3] and refs. therein); this difference will be apparent from charge density analysis hereafter.

ThCo crystallizes in the orthorhombic space group *Cmcm* [7], similar to *A*Ni and $ANiH_x$ [1,2]. To the best of our knowledge there are no reports on the structure and atomic positions for $ThCoH_4$, especially for hydrogen. In fact, for this purpose it is often required to replace hydrogen by deuterium for accurate determinations using neutron diffraction. It has been the aim of the present work to investigate the electronic structure of ThCo and $ThCoH_4$ because the effects of hydrogen insertion such as the changes of the electronic structure and both the strength and character of the chemical bonding are important for an understanding of the properties of the material. These effects are modeled herein within the well established quantum mechanical density functional theory (DFT) framework [8, 9].

Results and Discussion

Computational framework

Within DFT, we use projector augmented wave (PAW) potentials within the VASP academic code [10, 11], as built within the generalized gradient approximation (GGA) for an account of the effects of exchange and correlation [12]. Testing local density approximation (LDA) built potentials lead to largely smaller lattice parameters and volume magnitudes; the LDA which is constructed based on the electron gas distribution is known to be 'over binding'. Firstly, an optimization of the atomic positions and lattice para-

Cmcm	ThCo [7]	ThCo (calcd.)	Bader	$ThCoH_4$	Bader
Lattice parameters					
a, Å	3.74	3.68		3.85	
b, Å	10.88	10.86		11.70	
c, Å	4.15	4.04		4.70	
Volume, $Å^3$ / 2 fu	84.43	80.73		105.86	
Energy, eV	−30.241			−60.589	
Atomic positions					
Th 4*c* (0, *y*, 1/4)	0, 0.136, 1/4	0, 0.135, 1/4	+1	0, 0.131, 1/4	+1.8
Co 4*c* (0, *y*, 1/4)	0, 0.416, 1/4	0, 0.407, 1/4	−1	0, 0.403, 1/4	+0.04
H1 4*c* (0, *y*, 1/4)				0, 0.913, 1/4	−0.58
H2 8*f* (0, *y*, *z*)				0, 0.306, 0.503	−0.47
H3 4*b* (0, 1/2, 0)				0, 1/2, 0	−0.31
Shortest dist., Å					
Th–Co	2.86	2.76		3.06	
Th–H1/Th–H2/Th–H3				2.81/2.59/2.73	
Co–H1/Co–H2/Co–H3				1.93/1.63/1.64	

Table 1. Geometry optimization results as compared to experiment data for ThCo and calculated values for $ThCoH_4$.

meters is carried out. Then the equations of states (EOS) of ThCo and $ThCoH_4$ are obtained through energy-volume curves fitted with Birch EOS [13].

The calculated data are converged at an energy cut-off of 268 eV for all systems. The *k*-point integration is carried out with a starting mesh of $4 \times 4 \times 4$ up to $8 \times 8 \times 8$ for best convergence and relaxation to zero strains. The Brillouin zone integrals are approximated using a special *k*-point sampling following the Blöchl algorithm [14].

An analysis of the charge density results is possible by the approach of atoms in molecules and crystals (AIM) introduced by Bader [15] who developed an intuitive way of dividing molecules into atoms based purely on the electronic charge density. Typically in chemical systems, the charge density reaches a minimum between atoms, and this is a natural region to separate atoms from each other. Such an analysis can be useful when trends between similar chemical systems are examined [16].

Also, the changes brought in by hydrogen into the density of states are addressed together with the character of the chemical bond between two atomic constituents based on the crystal orbital overlap population (COOP) [17]. In the plots, positive, negative and zero COOP magnitudes are indicative of bonding, antibonding, and nonbonding interactions, respectively.

Geometry optimization

Using the crystal data of Florio *et al.* [7] for ThCo, a geometry relaxation was carried out. Within space group *Cmcm*, there are 4 formula units (fu) per cell, but due to the *C*-centering only two fu are explicitly accounted for in the calculations. Table 1 shows the experimental and calculated lattice parameters. The latter

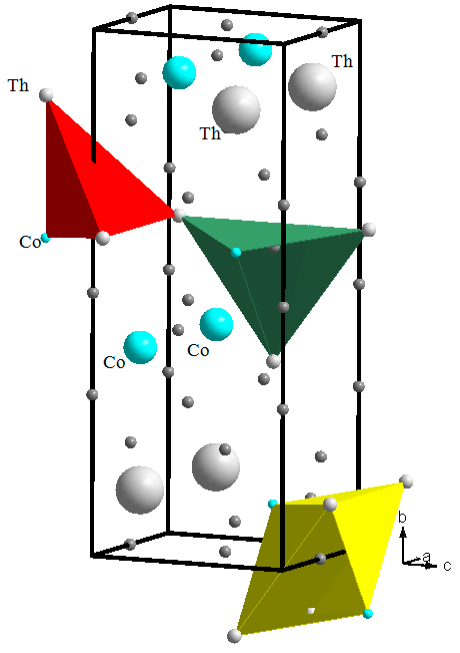

Fig. 1 (color online). Sketch of the proposed $ThCoH_4$ structure with coordination polyhedra of H1 (green, trigonal prism), H2 (red, tetrahedron) and H3 (yellow, flattened octahedron). Th and Co atoms are shown with smaller radii when taking part in the polyhedra.

are in fair agreement with the experiment especially for the atomic positions of Th while Co shows a change of the *y* coordinate. The volume is calculated slightly smaller, but the overall agreement gave confidence to investigate the hydrogenated system $ThCoH_4$.

For the hydrogenated *A*Ni compounds in space group *Cmcm* [18], the uptake of 3 hydrogen atoms per fu results in an isotropic expansion of the cell, and hydrogen atoms are dispatched over two crystallograph-

ically different sites, called hereafter H1 and H2. *RE*, Ni and H1 are at 4*c* positions and H2 at 8*f* (*cf.* Table 1). H1 and H2 are then found in A_3Ni_2 trigonal bipyramids and A_3Ni tetrahedra, respectively. When extra hydrogen (H3) is inserted, resulting in the $ANiH_4$ composition, Yaropolov *et al.* [2] proposed the occupation of the 4*b* (0,1/2,0) position whereby H3 is located in a A_4Ni_2 polyhedron. This is depicted in Fig. 1 for the presently studied system, *i. e.*, with *A* = Th and Ni replaced by Co. These starting atomic positions were used to optimize the structure of $ThCoH_4$. The proposition of H3 at 4*b* (0,1/2,0) was validated *versus* another *ad hoc* position, 4*a* (0,0,0), within preliminary calculations. The results led to a destabilization of the system by ∼3 eV when hydrogen is at the 4*a* position as compared to the 4*b* position. Therefore we adopted the latter for H3 in the following calculations.

After geometry optimization, the orthorhombic symmetry was kept for the hydrogenated system within space group *Cmcm*. The calculated values of the lattice parameters and the internal atomic coordinates are given in Table 1. The volume increase upon hydrogenation of ThCo is ∼ 25 %, a value within the range of $ANiH_4$, 23 – 25 % [2]. With respect to literature, the y_{Th} coordinate changes less than the y_{Co} and H1 and H2 coordinates. This is probably connected with the stronger bonding of H with Co rather than with Th resulting from larger distance to all three hydrogen sites, as shown in Table 1. The trend d(Co–H1) > d(Co–H2/H3) was also observed in hydrogenated CeNi and YNi [19,20]. Regarding the energies, the hydrogen uptake stabilizes ThCo by −15.2 eV for 4H. This is further analyzed in the context of the binding energies below.

Energy – Volume EOS

In order to establish energy and relative stability trends, the equation of state (EOS) is needed, since one cannot rely solely on the quantities obtained from plain lattice optimizations, especially when comparisons of energies and of volumes are required for different phases. The calculated total energy corresponds to the cohesion in the crystal, because the solution of the Kohn-Sham DFT equations gives the energy with respect to infinitely separated electrons and nuclei. As the zero of energy depends on the choice of the pseudopotentials, the energy becomes arbitrary through its shifting, not scaling. However, the energy derivatives as well as the EOS remain unaltered. For this reason one needs to establish EOS's from which the fit parameters are extracted for an assessment of the equilibrium values. This can be done from a set of $E(V)$ calculations for ThCo and $ThCoH_4$. The resulting curves shown in Fig. 2 have a quadratic variation which can be fitted with a Birch EOS to the 3rd order [13]:

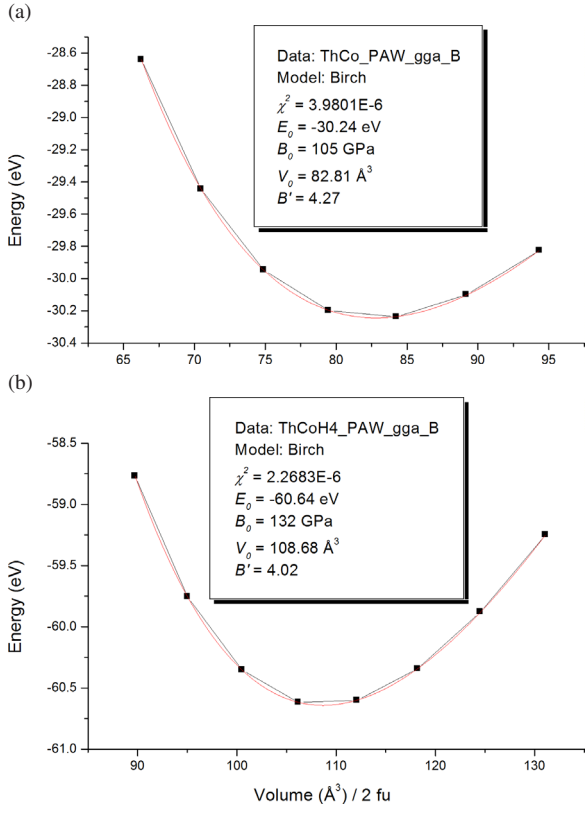

Fig. 2 (color online). Energy *versus* volume curves for a) ThCo and b) $ThCoH_4$ and fit results from Birch EOS shown in red. Low χ^2 magnitudes indicate the goodness of fit value.

$$E(V) = E_o(V_o) + \frac{9}{8} V_o B_o [(V_o/V)^{2/3} - 1]^2 + \frac{9}{16} B_o (B' - 4) V_o [(V_o/V)^{2/3} - 1]^3 \quad (1)$$

where E_o, V_o, B_o, and B' are the equilibrium energy, the volume, the bulk modulus, and its pressure derivative, respectively. In both panels the goodness of fit of χ^2 is $\sim 10^{-6}$, providing reliability to the fit values. The B' value amounts to ~ 4, a magnitude usually observed [19, 20]. The equilibrium volume of ThCo is close to the values calculated from geometry optimization and in better agreement with the experiment. For $ThCoH_4$, the equilibrium volume is slightly smaller than the optimized value. However,

fit values which are zero pressure equilibrium quantities should be considered as more reliable for the reasons above. The bulk modulus B_0 of ThCo amounts to ~ 105 GPa. Compared to other 1 : 1 intermetallics, this value is larger than for CeNi (77 GPa) [19] and YNi (85 GPa) [20] while Ni and Co have the same magnitude of bulk modulus (180 GPa). The observed trend may follow from the *A* elements adjoined to them, *i. e.* Ce (22 GPa), Y (41 GPa) and Th (54 GPa) [20]. A larger magnitude is obtained for $ThCoH_4$ despite the volume expansion, which could be related to the presence of metal-hydrogen bonding, especially Co–H, leading to an enhanced resistance of the system against compression and shearing. This is also observed for the hardening of carbides and borides.

Binding energies and charge density analysis

From the equilibrium energy results we examined the stability of $ThCoH_4$ using the following expression per fu: $E_{\text{stabil.}} = E(ThCoH_4) - E(ThCo) - 2\,E(H_2)$. While the first two terms of the right hand side of the equation are the equilibrium values obtained from the calculations, $E(H_2)$ is derived from PAW-GGA calculations of H in a cube box with a large lattice spacing of 5 Å. The resulting energy $E(H_2) = -6.59$ eV is the total electronic energy. It includes twice the energy of monohydrogen (-0.95 eV from similar calculations), and it needs to be corrected by the zero point energy (ZPE). For H_2, ZPE amounts to ~ 0.28 eV as calculated by the same method [21]. The binding energy of H_2 is then -4.41 eV which is close in magnitude to the dissociation energy (inverse sign) of the molecule as obtained from fluorescence excitation spectroscopy: ~ 36118 cm^{-1}, *i. e.* ~ 4.48 eV [22]. Then, with $E(H_2)$ and the equilibrium energy values, the stabilization energy of hydrogen in $ThCoH_4$ (per 2 fu, using equilibrium values in the inserts) is: $E_{\text{stabil.}}(H) = -60.64 - (-30.24) - 4(-6.59) = -4.04$ eV for all 8H, *i. e.* -0.5 eV per H. This value is close to the one computed for $YNiH_4$ of ~ -0.56 eV per H [20].

This is further quantified by the charge density analysis within the atoms in molecules (AIM) theory [15] presented above. In ThCo used as a reference for comparison, we compute a charge transfer of ~ 1 electron from Th towards Co (Table 1, Bader columns). This follows the electronegativity order (Ξ) on the Pauling scale [23], *i. e.* a less electronegative Th ($\Xi = 1.3$) with respect to Co ($\Xi = 1.9$) and a larger electronegativity for hydrogen: Ξ (H) = 2.2. When H enters ThCo, the charge on Th becomes larger ($+1.8$) and that on cobalt is not far from neutrality. The negative charges are carried by hydrogen atoms which are the nearest neighbors (*nn*) to cobalt, with different magnitudes ranging from -0.58 (H1) to -0.47 (H2) and -0.31 (H3). This indicates a range of iono-covalently to covalently bonded hydrogen which follows the number of Co nearest neighbors and Th next nearest neighbors to hydrogen in the coordination spheres, *i. e.*, Th3Co2, Th4Co2 and Th3Co, respectively. It can be seen that the difference of chemical behavior between the hydrogen atoms belonging to the two cobalt-containing polyhedra, namely Th3Co2 and Th4Co2, arises from the larger number of Th in the latter. This is different from ionic hydrides like MgH_2, where hydrogen is strongly bonded and carries a charge of ~ -1 (*cf.* [3] and refs. therein). Hence, it can be suggested that in $ThCoH_4$ hydrogen should desorb site-selectively from the intermetallic matrix, starting with the least ionically bonded H3, such as by the effect of temperature. The overall chemical picture is close to a complex-type system: $Th^{\delta+}(CoH_4)^{\delta-}$ with $\delta \sim 1.8$. Nevertheless, this charge transfer remains far from that in the ionic complex hydridocobaltate anion $(CoH_5)^{4-}$, in Mg_2CoH_5 which follows the 18-electron rule [24]. This is due to the largely electropositive character of Mg leading to a total charge transfer of 4 (2×2) electrons to CoH_5.

Density of states and chemical bonding

The site-projected density of states (PDOS) is shown in Fig. 3 for ThCo and $ThCoH_4$. Along the *x* axis the energy reference is taken with respect to the Fermi level E_F because both systems have a finite, albeit small, density of states at the top of the valence band (VB), with contributions arising from Th (*d,f*) and Co (*d*) states. The VB is mainly dominated by Co (*d*) states centered below E_F due to Co having its 3*d* subshell largely populated. On the contrary, the conduction band (CB, above E_F) is dominated by Th (5*f*) states. Nevertheless, itinerant states arising from Th (6*d*) are found within the VB; they are involved with the bonding involving Co valence states.

The similar peak shapes observed through the lower part of the VB indicate a quantum mixing between the metal constituents in the range $\{-6, -3$ eV$\}$ for ThCo and $\{-3$ eV, $E_F\}$ for $ThCoH_4$. In the latter, a narrowing for both Co and Th energy intervals within the VB is observed, accompanied by more localized and intense peaks, especially for cobalt. These are the

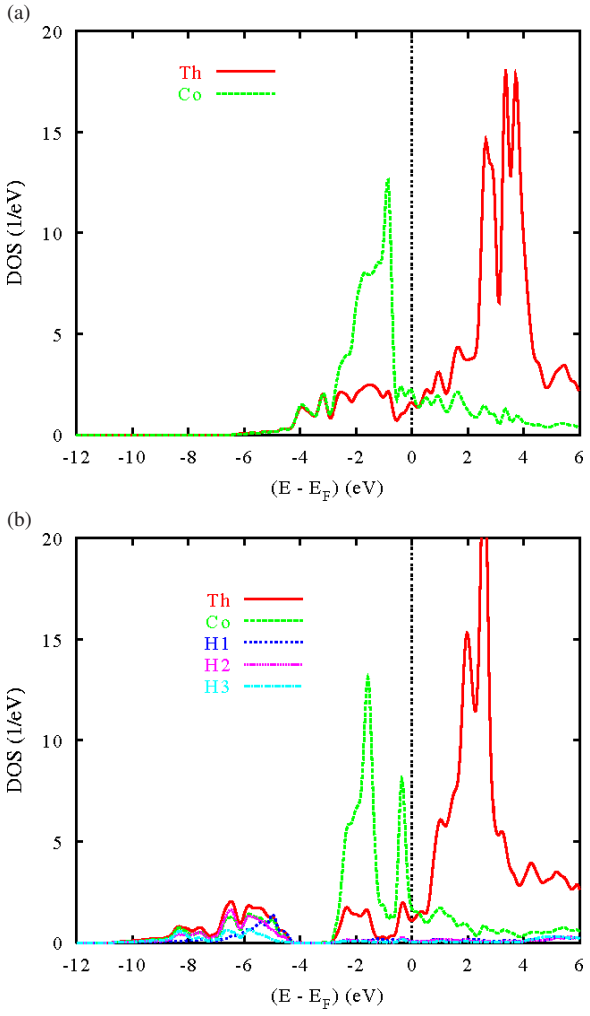

Fig. 3 (color online). Site-projected density of states for a) ThCo and b) $ThCoH_4$.

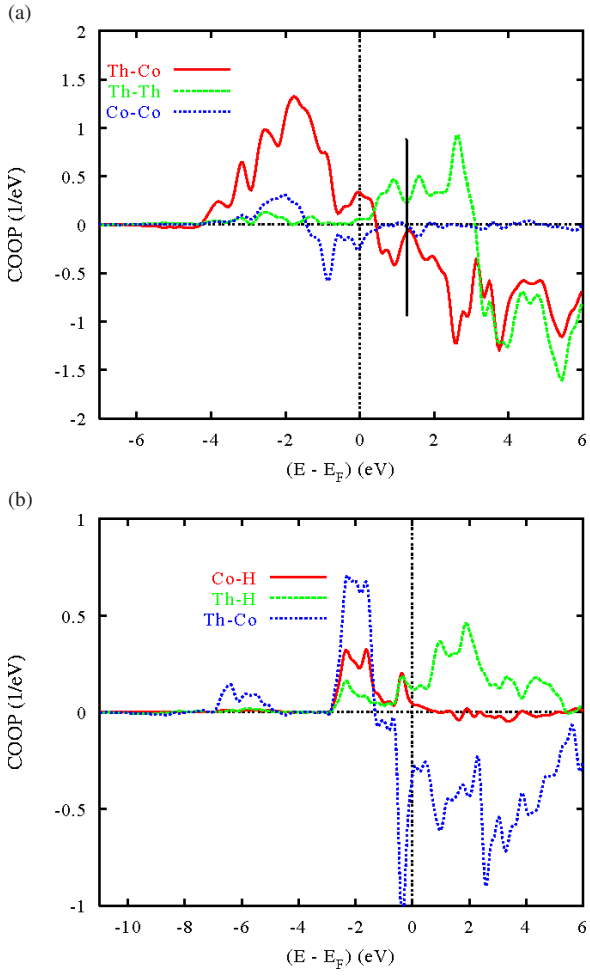

Fig. 4 (color online). Chemical bonding for pair interactions in a) ThCo and b) $ThCoH_4$.

respective consequences of the volume increase leading to larger interatomic separations and PDOS peak localization and of the extra electrons brought by the four additional hydrogen atoms. The novel feature of the PDOS with respect to ThCo is the emergence of extra states created in the lower part of the VB, *i. e.* between −4 eV and −10 eV within which hydrogen binds with the metallic constituents, mainly Co. This is also evident from the presence of Co and Th PDOS peaks just below E_F in Fig. 3b, involving the bonding of Co and Th *d* orbitals with H as detailed below.

The chemical bonding is discussed based on the COOP plots for metal-metal and metal-H interactions in Fig. 4. For a clear presentation of bonding strengths of the Th–H and Co–H interactions regroup all three sites H1, H2 and H3. In ThCo (Fig. 4a), the Th–Co interaction is stronger than Th–Th and Co–Co interactions. It is of bonding character over the whole VB energy range. This is also observed for the weaker Th–Th interactions. On the contrary, Co–Co shows bonding and antibonding interactions within the VB due to the high filling of Co (*d*) orbitals. The antibonding COOP appears in the CB at 1 eV for Th–Co and 3 eV for Th–Th. The energy order for the occurrence of antibonding COOP in ThCo is Co–Co at −1 eV, Th–Co at 1 eV and Th–Th at 3 eV. It is concomitant with the number of electrons involved in the interaction: the more electrons are involved, the earlier the antibonding COOPs appear.

In $ThCoH_4$ (Fig. 4b), the Th–Co bonding intensity is reduced with respect to Fig. 4a, it extends over a wider

energy range with a small intensity COOP centered at −7 eV, and it is separated from the major COOP contribution at −2 eV. Th–Co bonding remains dominant with respect to both Th–H and Co–H whose COOPs follow the same shape as Th–Co, signaling covalent-like interactions. Contrary to Fig. 4a, Th–Co antibonding COOPs in Fig. 4b are now observed below E_F. With respect to ThCo, the addition of four hydrogen atoms bringing four extra electrons leads to a higher energy shift of E_F as schematized by the bold vertical line at ∼ 1 eV in Fig. 4a. The enhancement of the antibonding COOP below E_F, signaling a less bonded Th–Co metal sublattice, is due to the larger Th–Co distance (Table 1) and to the involvement of some of the Th and Co electrons with hydrogen bonding. As in the PDOS plots, the COOP present a more localized feature due to the lager volume of the hydrogenated compound (Table 1). Although both metal-hydrogen interactions are bonding, the Th–H COOP intensity is much smaller than that of Co–H, being observed below the Th–Co COOP peaks at ∼ −2 eV. This supports the discussion above conclusion regarding the chemical structure. Both possess a COOP massif just below E_F, corresponding to the extra PDOS peak developed in $ThCoH_4$ (Fig. 3b).

Conclusion

The aim of this work using DFT electronic structure methods was to address the changes brought by the insertion of hydrogen into ThCo leading to the formation of the experimentally observed $ThCoH_4$. Full geometry optimizations lead to a positioning of hydrogen atoms within the intermetallic matrix. The energy volume equations of states for the intermetallic and the hydrogenated compound indicate its stabilization. The analyses of the DOS show large changes within the valence band with new states introduced by hydrogen into the lower part of the valence band and a larger localization of Th and Co partial DOS. From the chemical bonding analysis, the major bonding is observed for Co–H with antibonding Th–H. Bader charge analysis shows that hydrogen exhibits iono-covalent to covalent behavior. The overall chemical picture shows a positively charged $Th^{\delta+}$ and a complex hydridocobaltate $[CoH_4]^{\delta-}$ with $\delta = 1.8$, less ionic than in Mg-based hydridocobaltate.

[1] J.-L. Bobet, E. Grigorova, B. Chevalier, M. Khrussanova, P. Peshev, *Intermetallics* **2006**, *14*, 208.
[2] Y. L. Yaropolov, B. N. Verbetsky, V. A. Somenkov, *Proceedings of Hydrogen Materials Science and Chemistry of Carbon Nanomaterials*, ICHMS, Yalta, Ukraine **2009**, pp. 192 – 193.
[3] S. F. Matar, *Prog. Solid State Chem.* **2010**, *38*, 1.
[4] W. L. Korst, Technical Report NAA-SR-6881, Atomics International, Div. of North American Aviation, Inc., Canoga Park, Calif., USA **1962**.
[5] K. H. J. Buschow, H. H. Van Mal, A. R. Miedema, *J. Less-Common Met.* **1975**, *42*, 163.
[6] J.-G. Roquefere, S. F. Matar, J.-L. Bobet, *Int. J. Hydrogen Energy* **2010**, *35*, 7858
[7] J. V. Florio, N. C. Baezinger, R. E. Rundle, *Acta Crystallogr.* **1957**, *9*, 367.
[8] P. Hohenberg, W. Kohn, *Phys. Rev.* **1964**, *136*, 864.
[9] W. Kohn, L. J. Sham, *Phys. Rev*. **1965**, *140*, 1133.
[10] G. Kresse, J. Furthmüller, *Phys. Rev. B* **1996**, *54*, 11169.
[11] G. Kresse, J. Joubert, *Phys. Rev. B* **1999**, *59*, 1758.
[12] J. Perdew, K. Burke, M. Ernzerhof, *Phys. Rev. Lett.* **1996**, *77*, 3865.
[13] F. Birch, *J. Geophys. Res.* **1978**, *83*, 1257.
[14] P. E. Blöchl, *Phys. Rev. B* **1994**, *50*, 17953.
[15] W. Tang, E. Sanville, G. Henkelman, *J. Phys.: Condens. Matter* **2009**, *21*, 084204.
[16] S. F. Matar, A. Largeteau, G. Demazeau, *Solid State Sci*. **2010**, *12*, 1779.
[17] R. Hoffmann, *Angew. Chem.* **1987**, *99*, 871; *Angew. Chem., Int. Ed. Engl.* **1987**, *26*, 846.
[18] S. W. Peterson, V. N. Sadana, W. L. Korst, *J. Phys. (Paris)* **1965**, *25*, 451.
[19] S. F. Matar, *Solid State Sci.* **2010**, *12*, 59.
[20] S. F. Matar, M. Nakhl, A. F. Al Alam, N. Ouaini, B. Chevalier, *Chem. Phys.* **2010**, *377*, 109.
[21] O. I. Velikikhatnyi, P. N. Kumta, *Mater. Sci. Eng. B* **2007**, *140*, 114.
[22] A. Balakrishnan, V. Smith, B. P. Stoicheff, *Phys. Rev. Lett.* **1992**, *68*, 2149.
[23] L. Pauling, *The Nature of the Chemical Bond*, 3rd ed., Cornell University Press, Ithaca, NY **1960**, pp. 88 – 107.
[24] J. N. Chotard, Y. Filinchuk, B. Revaz, K. Yvon, *Angew. Chem.* **2006**, *118*, 7934; *Angew. Chem. Int. Ed.* **2006**, *45*, 7770.